Electrocatalytic Oxidation of Glycerol Using Solid-State Synthesised Nickel Boride: Impact of Key Electrolysis Parameters on Product Selectivity

Ann Cathrin Brix,[a] Dulce M. Morales,[b] Michael Braun,[c] Daliborka Jambrec,[a] João R. C. Junqueira,[a] Steffen Cychy,[d] Sabine Seisel,[a] Justus Masa,[e] Martin Muhler,[d] Corina Andronescu,*[c] and Wolfgang Schuhmann*[a]

Water electrolysis is a promising technology for sustainable hydrogen production; however, its commercialisation is limited by sluggish kinetics of the oxygen evolution reaction (OER). A potential alternative to the OER is hence required and is seen in the electrocatalytic glycerol oxidation reaction (GOR) as it offers concomitant value-added product generation from a cheap and abundant feedstock. Here, we show a facile solid-state synthesis method to obtain Ni-boride, a non-noble metal-based catalyst subsequently used in an in-depth study of the GOR product distribution as a function of key electrolysis parameters. Highly crystalline, mixed-phase Ni borides were obtained, and their synthesis was successfully optimised regarding GOR activity. Long-term chronoamperometry was conducted in a circular flow-through cell and samples were analysed by HPLC. It is shown that the formation of lactic acid, one of the most valuable GOR products, can be enhanced by optimising the electrolyte composition and the applied potential.

1. Introduction

Energy generation via fossil fuels, a limited resource, has led to detrimental environmental issues such as pollution and climate change due to CO_2 emissions. The future renewable energy infrastructure, therefore, requires clean and sustainable hydrogen production, for instance, by electrocatalytic processes. The water electrolysis technology conventionally features the formation of hydrogen as the cathode reaction, whereas usually the oxygen evolution reaction (OER) is the anode reaction. The latter poses the limiting factor for large-scale commercialisation as high energy input is needed to overcome its sluggish kinetics. Alternative anode reactions could offer a viable solution as the high energy cost could be mitigated by concomitantly converting a cheap and abundant feedstock into value-added products. Glycerol is a major by-product of biodiesel manufacturing and can be oxidised to many valuable compounds including lactic acid, which has a wide range of industrial applications.[1] Dihydroxyacetone (DHA), mesoxalic acid and tartronic acid are also possible glycerol oxidation products which find application in cosmetics[2] or are of medicinal and industrial value.[3] However, it is rather difficult to selectively form such partially oxidised products as large amounts of formic acid are easily obtained from multiple pathways featuring C–C bond cleavage or, in an even more unfavourable case, the oxidation is directly leading to the formation of CO_2.[4] Materials based on noble metals such as Pt,[5,6] Au[6,7] or Pd[8] and corresponding bimetallic alloys[9,10] have been proposed as catalysts for the glycerol oxidation reaction (GOR), often in acidic media. However, these metals are scarce and, while they catalyse the GOR at low potentials, they face challenges such as low current densities due to strong CO poisoning or the formation of metal oxides. Hence, abundant and cheap non-noble metal-based catalysts containing e.g. Ni and Co would be much more favourable as they are less prone to CO poisoning.[11] Furthermore, they are stable in alkaline media where higher reaction rates are achieved for the oxidation of alcohols.[6] However, only a few studies about this kind of material are available[12,13] and even fewer include detailed product analysis exploring selectivity optimisation towards a certain valuable product.[14,15] Combinations of such

[a] A. C. Brix, Dr. D. Jambrec, J. R. C. Junqueira, Dr. S. Seisel, Prof. Dr. W. Schuhmann
Analytical Chemistry – Center for Electrochemical Sciences (CES), Faculty of Chemistry and Biochemistry
Ruhr University Bochum
Universitätsstraße 150, 44780 Bochum, Germany
E-mail: wolfgang.schuhmann@rub.de
[b] Dr. D. M. Morales
Nachwuchsgruppe Gestaltung des Sauerstoffentwicklungsmechanismus
Helmholtz-Zentrum Berlin für Materialien und Energie GmbH
Hahn-Meintner-Platz 1, 14109 Berlin, Germany
[c] M. Braun, Prof. Dr. C. Andronescu
Technical Chemistry III and CENIDE Center for Nanointegration, Faculty of Chemistry, University of Duisburg-Essen
Carl-Benz-Straße 199, 47057 Duisburg, Germany
E-mail: corina.andronescu@uni-due.de
[d] S. Cychy, Prof. Dr. M. Muhler
Laboratory of Industrial Chemistry, Faculty of Chemistry and Biochemistry
Ruhr University Bochum
Universitätsstr. 150, 44780 Bochum, Germany
[e] Dr. J. Masa
Max-Planck-Institute for Chemical Energy Conversion (MPI-CEC)
Stiftstraße 34–36, 45470 Mülheim an der Ruhr, Germany

Supporting information for this article is available on the WWW under https://doi.org/10.1002/celc.202100739

transition metals with non-metals such as B, N, S, Se and P have attracted great interest as highly active catalysts for the hydrogen evolution reaction (HER) and the OER, nickel boride (Ni_xB)[16] in particular. The latter has also shown to be active towards 5-(hydroxymethyl)furfural (HMF),[17] methanol,[18] ethanol and ethylene glycol oxidation,[19] rendering it an interesting material for anode reactions alternative to the OER. Most commonly, M_xB-type catalysts are synthesised via a wet chemical reduction method that involves the use of toxic salt precursors such as Ni chloride and requires a post-annealing step to produce active catalyst materials. Therefore, synthesis methods that require less hazardous materials to obtain these catalysts should be considered.

Here, we propose a comparatively facile and easily scalable solid-state synthesis method avoiding a tedious synthesis via highly toxic and pyrophoric precursors and intermediates to obtain Ni borides and show the optimisation of annealing temperature, Ni:B ratio and Ni precursor particle size. During a subsequent detailed product analysis study we could detect lactic acid which has previously only been reported once for a non-noble metal-containing Ni-based electrocatalyst.[20] We could selectively influence the amount of lactic acid formed by a rational approach of modulating electrolyte composition and applied potential, which, to the best of our knowledge, has not been demonstrated before.

2. Results and Discussion

Ni_xB catalyst powders were synthesised by means of a high-temperature solid-state approach using Ni powders with either a particle size in the micron (Ni-µm) or in the nanometre (Ni-nm) range as precursor. The mixtures contained Ni:B ratios of 2:1 or 3:1 and were annealed at different temperatures (300, 600 and 1000 °C) under inert atmosphere (see SI experimental). The resulting catalysts are labelled accordingly e.g. Ni_xB-nm-2:1-600 denominates the material prepared using the Ni-nm precursor mixed with B at a ratio of 2:1 and annealed at 600 °C. SEM micrographs are shown in Figure SI1 and the presence of Ni, B and O in the obtained catalysts was confirmed by EDX spectroscopy, the latter being attributed to spontaneous oxidation in air (cf. Figure SI2). Elemental mapping (cf. Figure SI3) shows that Ni and B are present within a Ni_xB particle. Typical cyclic voltammograms (CV) of the obtained Ni_xB materials recorded in 1 M KOH in the presence (red curve) and in the absence (black curve) of 0.1 M glycerol are displayed in Figure 1.

The characteristic $Ni^{2+} \rightarrow Ni^{3+}$ oxidation peak is observed at a potential of about 1.40 V vs. RHE in the absence of glycerol and the corresponding reduction peak at approximately 1.34 V vs. RHE.[13,21] For the OER a significant current density increase is recorded at potentials exceeding 1.5 V as the OER requires the formation of NiOOH.[22] After addition of glycerol, no distinct Ni oxidation peak is observed as the glycerol oxidation reaction (GOR) seems to be initiated as soon as minor Ni^{2+} oxidation takes place. At potentials above 1.53 V vs. RHE a change in the current slope is observed, most likely due to an increasing

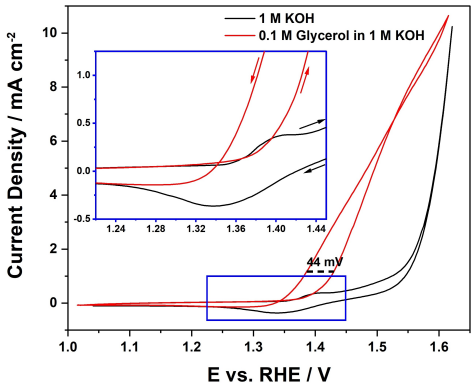

Figure 1. Cyclic voltammograms recorded in 1 M KOH solution in the absence (black) and presence (red) of 0.1 M glycerol. Voltammograms were recorded at a scan rate of 10 mV s^{-1} with an electrode rotation of 1600 rpm (sample: Ni_xB-µm-3:1-600).

contribution of the OER. The large potential gap between the curves recorded in absence and presence of glycerol can be explained by the adsorption characteristics of oxidised Ni surfaces as they bind OH* species very strongly. While the resulting high OH* coverage is highly favourable for alcohol oxidation, the binding energy of the reaction intermediates is too strong for the OER.[23] Hence, the electrode processes are likely governed by competitive adsorption of glycerol and OH^- with a coverage strongly dependent on the applied potential.

The influence of three key synthesis parameters, namely the annealing temperature, the Ni-to-B ratio and the particle size of the Ni precursor on the electrocatalytic activity in the GOR (Figures 2a, 2c and 2e, respectively) and on the crystallinity and phase composition of the samples (Figures 2b, 2d and 2f, respectively) was investigated. As shown in Figure 2a, the voltammetric responses of catalysts prepared using Ni-µm with a Ni:B ratio of 2:1 at 300, 600 and 1000 °C indicate that neither too low nor too high annealing temperatures improve the catalysts' GOR activity. XRD patterns of the as-synthesised materials revealed highly crystalline mixed phases. While the diffractogram of the sample annealed at 300 °C matches that of elemental Ni, Ni_3B reflections start to emerge at 600 °C and increase in intensity with increasing temperature. At 1000 °C, minor contributions of Ni_2B were also observed. However, ICP-MS measurements (cf. Table SI1) confirm the presence of B in the samples in the same relative amount as aimed for in the synthesis. Thus, excess B may be present in an XRD-amorphous phase. The conversion of Ni into its borides increases with increasing annealing temperature (Figure 2b). The sample obtained at the highest temperature exhibits lower activity in the GOR possibly due to increased sintering at high temperatures. In order to evaluate the effect of the Ni:B ratio, Ni_xB-µm-600 samples with Ni:B ratios of 2:1 and 3:1 as well as the pristine Ni-µm precursor were compared. Figure 2c suggests that an increase in the amount of B coincides with an increase in GOR activity in the order 1:0 < 3:1 < 2:1. The synthesis of Ni_xB catalysts at an annealing temperature of 600 °C and a Ni:B ratio of 2:1 was further optimised by using a Ni precursor with a particle size in the range of 100 nm (Ni-nm), considerably

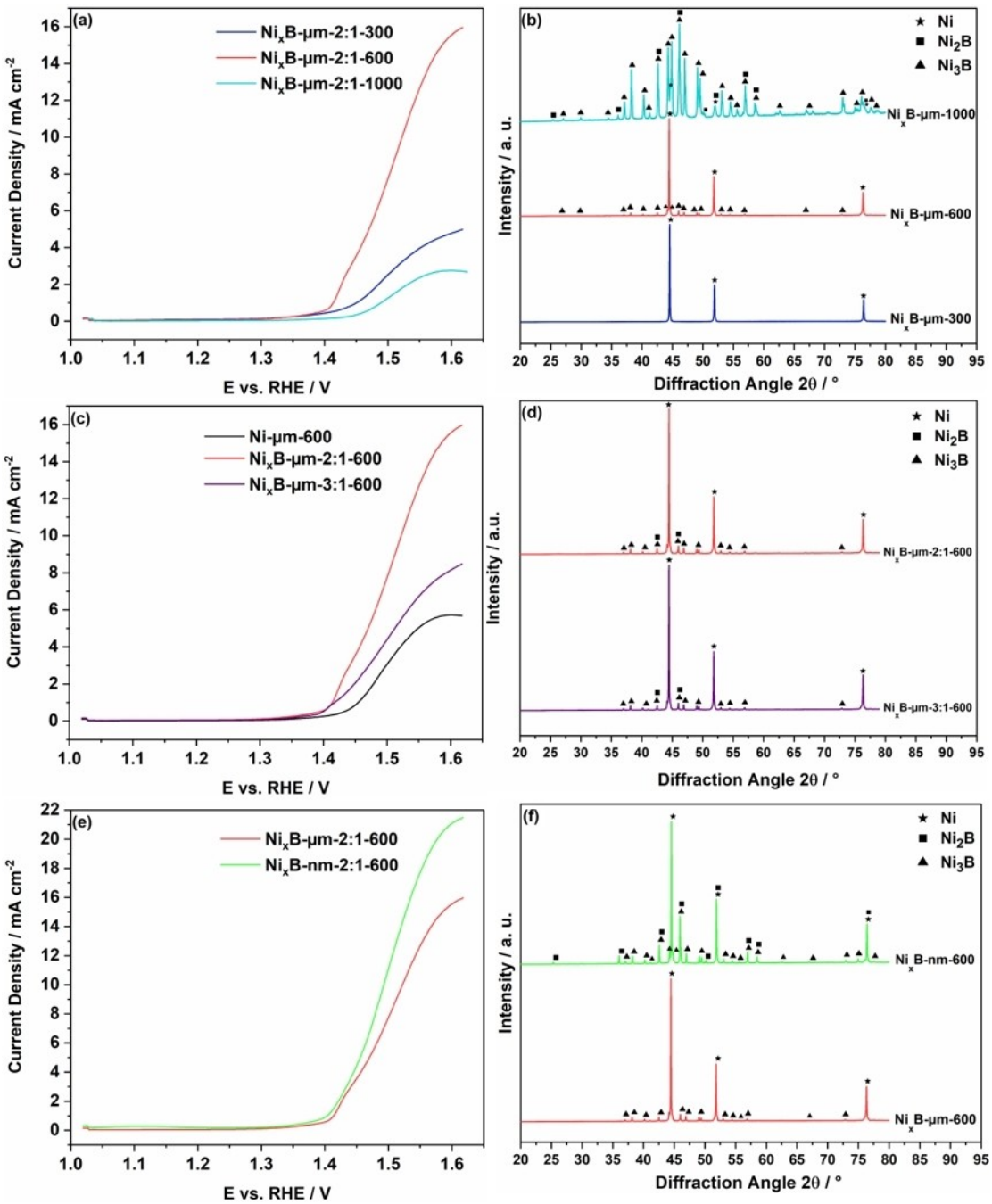

Figure 2. Influence of annealing temperature used for Ni$_x$B-µm-2:1 catalysts on (a) the voltammetric response and (b) their corresponding XRD patterns. (c) Voltammetric response showing the influence of the Ni:B ratio used for the synthesis of Ni$_x$B-µm samples annealed at 600 °C and (d) their corresponding XRD patterns (compared with Ni (★), Ni$_2$B (■) and Ni$_3$B (▲) as references). (e) Voltammetric response showing the influence of the particle size of the Ni precursor used for preparing Ni$_x$B samples with Ni:B ratio of 2:1 annealed at 600 °C and (f) their corresponding XRD patterns. Voltammograms were recorded at a scan rate 10 mV s^{-1} and 1600 rpm electrode rotation; 0.1 M glycerol in 1 M KOH.

smaller than the Ni-µm precursor, aiming at an increased surface-to-volume ratio. The obtained Ni$_x$B-nm-2:1-600 sample exhibited the highest current densities of all investigated samples (Figure 2e) and XRD patterns with a larger number of reflections (Figure 2f). This catalyst material was, thus, used in subsequent investigations regarding selectivity optimisation.

The reaction pathway scheme of the complex multi-step oxidation of glycerol (Figure 3a) shows that OH^- is involved in almost all reaction steps. Therefore, the pH value of the electrolyte as well as the local pH value at the site of the reaction most likely play a crucial role especially in favouring the non-electrochemical steps (the Cannizzaro reaction, in particular; cf. Figure 3b) that lead to the formation of lactic acid. As OH^- and glycerol supposedly adsorb competitively on the catalyst surface, product distributions may also be influenced by the glycerol concentration.[24]

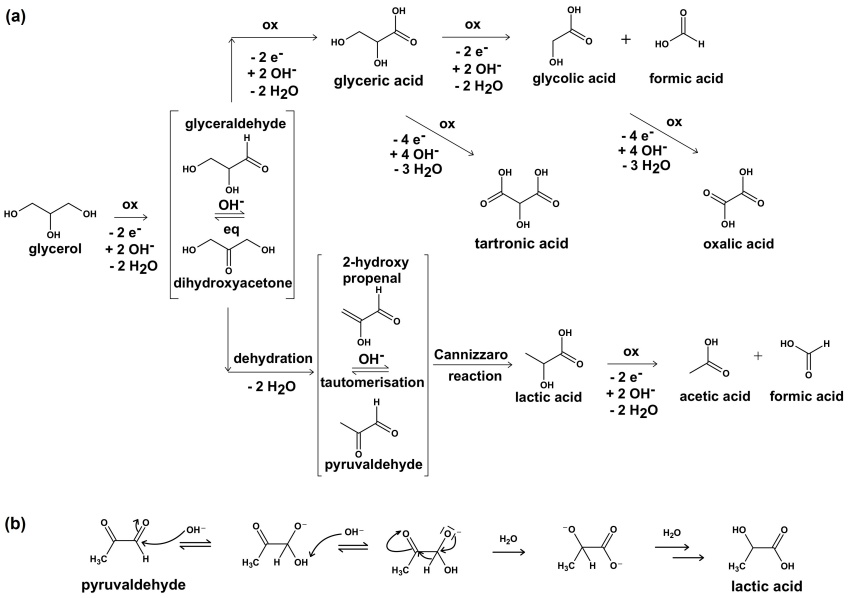

Figure 3. (a) Reaction pathways for electrocatalytic glycerol oxidation proposed in literature.[9,15] (b) Mechanism of intramolecular Cannizzaro reaction forming lactic acid.

Preliminary product distribution studies were conducted in an H-type electrochemical cell of which an image is provided in Figure SI4a. The cell has a volume of about 7 mL which allows the detection of reaction products even at low conversions. Using this setup, the impact of electrolyte composition on the selectivity was investigated as discussed in detail in the SI. Increasing the KOH concentration in the electrolyte was found to lead to an increase in the current densities which could be related to the increased electrolyte conductivity (cf. Figure SI5). Excluding formic acid, the highest concentrations for all products, which were determined by means of HPLC analysis, were found at a KOH concentration of 2 M (cf. Figure SI6), while with increasing glycerol concentration decreasing current densities were recorded (Figure SI7), which may be due to increased viscosity at higher glycerol concentration. This was confirmed by determining the diffusion coefficient of a model compound at a Pt microelectrode (cf. Figure SI7d and Table SI2).

The highest lactic acid concentration was detected at 0.5 M glycerol (cf. Figure SI8). The applicability of the optimised electrolyte composition found with short-time chronoamperometric tests in an H-cell was further studied using a circular flow-through electrolyser setup to take advantage of increased mass transport and the ability to take multiple samples during a longer measurement period from the anolyte reservoir. Its contents were continuously pumped through the working electrode compartment at a flow rate of 12 mL/min during chronoamperometric measurements conducted for 24 h. An image of the setup is provided in the supporting information (cf. Figure SI4b). The applied potentials are reported with respect to the Ag/AgCl/KCl (3 M) reference electrode.

Firstly, the Ni_xB-nm-2:1-600 catalyst was investigated with the electrolyte composition used initially for RDE measurements (0.1 M glycerol in 1 M KOH). High degrees of conversion and, hence, strong decay in current density were observed. Subsequently, chronoamperometry was recorded in electrolyte with the optimal concentration as found in preliminary experiments, namely 0.5 M glycerol in 2 M KOH. The corresponding chronoamperograms are shown in Figure 4a (dark green for 0.1 M glycerol in 1 M KOH and light green for 0.5 M glycerol in 2 M KOH). During the 24 h chronoamperometry measurement at

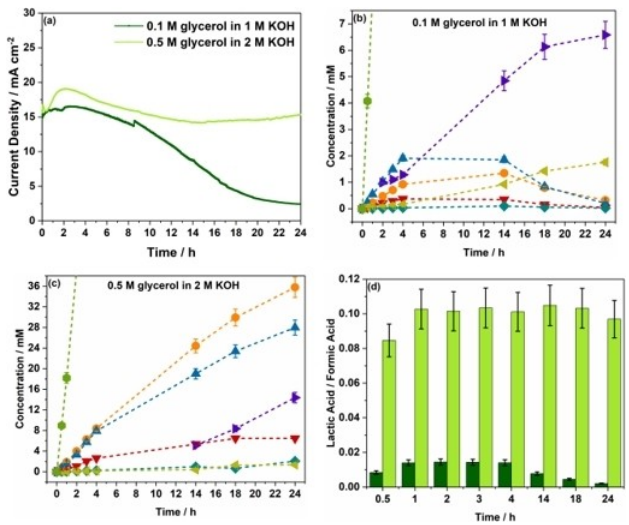

Figure 4. Effect of electrolyte composition during 24 h chronoamperometry at 0.5 V vs. Ag/AgCl/KCl (3 M) comparing 0.1 M glycerol/1 M KOH (dark green) and 0.5 M glycerol/2 M KOH (light green). (a) Chronoamperometric response. Product concentrations were analysed by HPLC from electrolyte sampled at different times in (b) 0.1 M glycerol in 1 M KOH and (c) 0.5 M glycerol in 2 M KOH. (d) Lactic acid to formic acid concentration ratios calculated based on data from (b) and (c) (orange ● and green ⬣). Products: lactic acid (orange ●), glycolic acid (blue ▲), glyceric acid (red ▼), tartronic acid (dark cyan ♦), acetic acid (yellow-green ◀), oxalic acid (purple ▶), formic acid (green ⬣). Dashed lines are guides for the eye.

0.5 V vs. Ag/AgCl/KCl (3 M) aliquots were taken at t = 0, 0.5, 1, 2, 3, 4, 14, 18 and 24 h and acidified immediately outside of the electrolysis cell with the same volume of 0.51 M sulfuric acid. Products identified by HPLC were formic acid, lactic acid, glycolic acid, glyceric acid, oxalic acid, as well as small amounts of tartronic acid and acetic acid. The corresponding chromatograms and the product concentrations including formic acid are displayed in Figure SI9. For the case of 0.1 M glycerol in 1 M KOH, product concentrations of most valuable compounds such as lactic acid, glycolic acid and glyceric acid increase initially with time, however, they decrease, subsequently, at longer electrolysis time (Figure 4b). Meanwhile, compounds such as oxalic acid, acetic acid and formic acid increase continuously, suggesting that after being generated they are not further oxidized at the electrode surface as long as more easily oxidisable compounds are present.

This depletion effect becomes clearly visible when a certain amount of glycerol has been converted leading to primary products being formed at a slower rate than that of their further conversion.

In the case of the optimised electrolyte composition (Figure 4c), much higher product concentrations were obtained indicating that the selectivity towards specifically lactic acid is favoured, which reaches concentrations of almost 40 mM under these conditions. The comparison between the ratio of lactic acid and formic acid concentrations for the two different electrolyte compositions is shown in Figure 4d, demonstrating further the clear differences between the two electrolyte compositions. For 0.5 M glycerol in 2 M KOH (light green) at all sampling times, the lactic acid to formic acid values are significantly and continuously higher than those obtained with 0.1 M glycerol in 1 M KOH.

To investigate the effect of the applied potential on the product distribution, the anode potential was varied between 0.4 and 0.6 V vs. Ag/AgCl/KCl (3 M) in increments of 50 mV. Figure 5a shows the corresponding chronoamperograms recorded for 24 h with the Ni_xB-nm-2:1-600 catalyst using 0.5 M glycerol in 2 M KOH as electrolyte. Higher potentials led to higher current densities at the beginning of the electrolysis due to a higher reaction rate, which is also observed in the corresponding conversion vs. time plots (Figure 5b). For the case of 0.6 V vs. Ag/AgCl/KCl (3 M), the high GOR rate led to a considerably large decrease in current density within the measuring time of 24 h, from nearly 60 mA/cm^2 at t = 0 to less than 30 mA/cm^2 at t = 24 h.

Product concentrations of lactic acid, glycolic acid and oxalic acid were low at potentials below 0.45 V vs. Ag/AgCl/KCl (3 M) (cf. HPLC data in Figure 6a and 6b) and steadily increasing over the complete duration of the measurement, however, still below 10 mM after 24 h. At 0.5 and 0.55 V vs. Ag/AgCl/KCl (3 M), much higher product concentrations were detected reaching over 40 mM for lactic acid. However, with the latter potential, the concentration increase of lactic acid already levels off between 18 and 24 h while the glycolic acid concentration decreased after 18 h (Figure 6c). For the highest applied potential of 0.6 V (Figure 6d), this effect of the depletion of some of the formed products such as lactic acid, glycolic acid, glyceric acid and tartronic acid at longer electrolysis times is even more pronounced and likely correlated with a higher conversion of glycerol, e.g. peaking at 14 h in the case of lactic acid with a concentration of about 30 mM. These findings support the hypothesis of a competition for the active sites at the catalyst surface and suggests that continuous flow-through

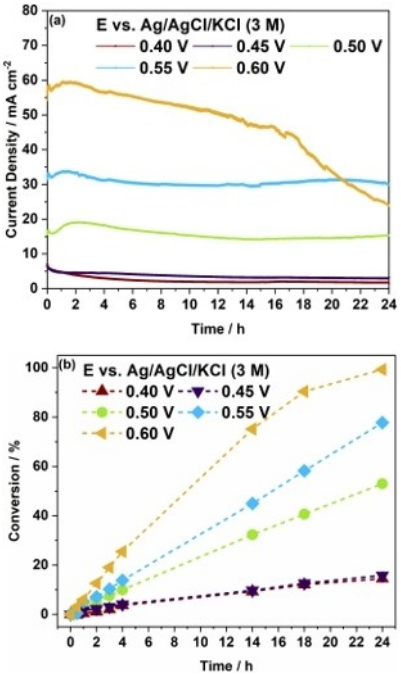

Figure 5. Effect of variation of applied potential on the conversion. (a) Comparison of chronoamperometric responses recorded using 0.5 M glycerol in 2 M KOH as electrolyte. (b) Comparison of conversion as a function of time. Dashed lines are guides for the eyes.

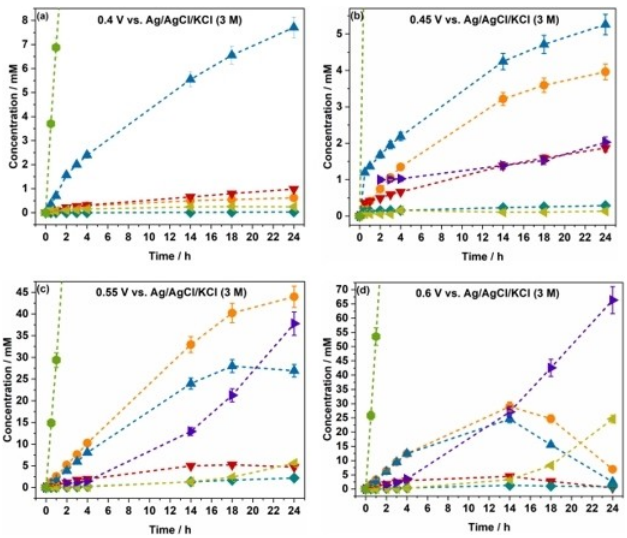

Figure 6. Product concentrations analysed by HPLC at different times during 24 h of chronoamperometry at different applied potentials (a) 0.4 V (b) 0.45 V (c) 0.55 V (d) 0.6 V vs. Ag/AgCl/KCl (3 M). Products: lactic acid (orange ●), glycolic acid (blue ▲), glyceric acid (red ▼), tartronic acid (dark cyan ♦), acetic acid (yellow-green ◀), oxalic acid (purple ▶), formic acid (green ⬣). Dashed lines are guides for the eyes.

reactors with comparatively low steady-state conversion are beneficial. The product concentrations as a function of electrolysis time are displayed in a scale adjusted for formation of formic acid in Figure SI10.

We focused our discussion primarily on the product concentrations as a direct means to evaluate the impact of different electrolysis parameters. For reference, the faradaic efficiencies after 14 and 18 h are provided in the supporting information (cf. Figure SI11).

Comparing the concentrations of all products detected by HPLC as a function of applied potential sheds light on which reaction pathway is favoured under which conditions, providing possible ways to tune the selectivity for a specific product. The formed products can be sorted into two categories (Figure 7).

Formic acid, oxalic acid and acetic acid are characterised by a continuous increase in concentration with increasing potential and the highest concentrations are recorded at the highest applied potential (0.6 V vs. Ag/AgCl/KCl (3 M)). This can be explained by the ongoing formation of these compounds from previously formed reaction intermediates containing carbon atoms with lower oxidation states, such as glycolic acid and lactic acid, via C–C bond scission. Additionally, their higher degree of oxidation may provide increased stability against further oxidation at this potential. Glyceric acid, glycolic acid, tartronic acid and lactic acid, on the other hand, are increasingly formed at lower potentials, but their concentrations decrease again at high potentials. For glyceric acid and glycolic acid, the highest concentrations were detected at 0.5 V vs. Ag/AgCl/KCl (3 M), which indicates that they are formed early during the measurement but are easily oxidised further. For lactic acid and tartronic acid, the highest concentrations were observed at slightly higher potential (0.55 V vs. Ag/AgCl/KCl (3 M)), which could be due to an increased stability as both molecules contain relatively stable functional groups such as carboxylic acid and methyl groups. The product with the highest concentration at a particular potential is indicative of which pathway is favoured in that case. At the comparably low potentials of 0.4 and 0.45 V vs. Ag/AgCl/KCl (3 M), glycolic acid is detected with the highest concentration, indicating that the pathway starting with the oxidation of glyceraldehyde to glyceric acid is favoured in this case. At medium potentials (0.5 and 0.55 V vs. Ag/AgCl/KCl (3 M)) lactic acid is formed the most via the alternative main pathway of the GOR reaction scheme (Figure 3). At the highest potential of 0.6 V vs. Ag/AgCl/KCl (3 M) oxalic acid is the predominant product supposedly due to its higher oxidation degree. Hence, the applied potential together with an optimized KOH concentration and avoiding depletion of glycerol can be advantageously used to selectively manipulate the reaction pathway to favour certain desired products of the GOR.

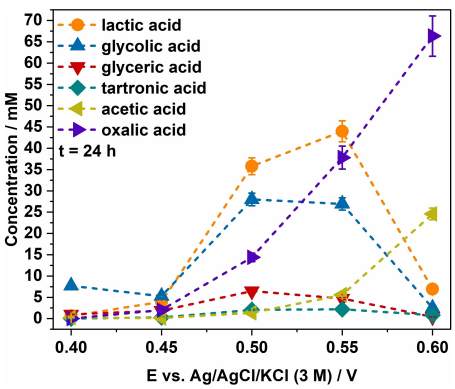

Figure 7. Product concentrations analysed by HPLC after 24 h of chronoamperometry as a function of different applied potentials. Products: lactic acid (orange ●), glycolic acid (blue ▲), glyceric acid (red ▼), tartronic acid (dark cyan ♦), acetic acid (yellow-green ◀), oxalic acid (purple ▶). Dashed lines are guides for the eyes.

Compared our results with previous accounts of Ni-based GOR electrocatalysts with comparable product analysis by HPLC (cf. Table SI3) the here proposed material exhibited medium activity, however, it demonstrated very good stability over 24 h, an extended period of electrolysis which is rarely reported. To the best of our knowledge, our findings feature the highest lactic acid selectivity reported to date with almost 9% at optimised electrolysis conditions.

3. Conclusions

A facile and easily scalable solid-state synthesis method to fabricate mixed-phase Ni boride catalysts for the GOR was demonstrated. XRD studies revealed highly crystalline mixed-phase Ni borides with different compositions as a function of the annealing temperature, Ni:B ratio, and particle size of Ni precursor. Optimal electrocatalytic activity was achieved by using a moderate annealing temperature (600 °C), increasing the B content to a Ni:B ratio of 2:1 and using nano-sized as opposed to micron-sized Ni precursor particles. Preliminary electrolysis using the best-performing catalyst (Ni_xB-nm-2:1-600) showed multiple compounds including formic acid, lactic acid, glycolic acid, glyceric acid, oxalic acid and acetic acid. Variation of electrolyte composition regarding glycerol and KOH concentrations indicated that lactic acid production can be increased by using 0.5 M glycerol in 2 M KOH. These findings were successfully applied in long-term electrolysis measurements highlighting the high stability of the catalyst within 24 h. Different reaction pathways were observed by applying different potentials between 0.4 and 0.6 V vs. Ag/AgCl/KCl (3 M). It was shown that the lactic acid concentration can be substantially increased by optimising the electrolyte composition and using mild potentials of around 0.5 to 0.55 V vs. Ag/AgCl/KCl (3 M).

Acknowledgements

This project was funded by the Deutsche Forschungsgemeinschaft (DFG, German Research Foundation) in the framework of the Research Unit 2982 "UNODE – Unusual Anode Reactions" [433304666 – WS, 433304702 – CA, 433305060 – MM]. The authors acknowledge the contribution of Sandra Schmidt for performing SEM and EDX measurements and Martin Trautmann

for performing ICP-MS measurements. Open access funding enabled and organized by Projekt DEAL.

Conflict of Interest

The authors declare no conflict of interest.

Keywords: electrocatalytic glycerol oxidation · nickel boride · alkaline electrolyte · flow-through cell · product analysis

[1] a) D. Garlotta, *J. Polym. Environ.* **2001**, *9*, 63–84; b) G. M. Lari, R. García-Muelas, C. Mondelli, N. López, J. Pérez-Ramírez, *Green Chem.* **2016**, *18*, 4682–4692; c) N. Razali, A. Z. Abdullah, *Appl. Catal. A* **2017**, *543*, 234–246.
[2] A. C. Garcia, Y. Y. Birdja, G. Tremiliosi-Filho, M. T. M. Koper, *J. Catal.* **2017**, *346*, 117–124.
[3] a) C.-H. C. Zhou, J. N. Beltramini, Y.-X. Fan, G. Q. M. Lu, *Chem. Soc. Rev.* **2008**, *37*, 527–549; b) E. Antolini, *Catalysts* **2019**, *9*, 980.
[4] L. Fan, B. Liu, N. Senthilkumar, G. Wang, Z. Wen, *Energy Technol.* **2021**, *9*, 2000804.
[5] a) S. Kongjao, S. Damronglerd, M. Hunsom, *J. Appl. Electrochem.* **2011**, *41*, 215–222; b) L. Roquet, E. M. Belgsir, J.-M. Léger, C. Lamy, *Electrochim. Act.* **1994**, *39*, 2387–2394; c) N. Worz, A. Brandner, P. Claus, *J. Phys. Chem. C* **2010**, *114*, 1164–1172; d) Y. Zhou, Y. Shen, J. Piao, *ChemElectroChem* **2018**, *5*, 1636–1643.
[6] Y. Kwon, K. J. P. Schouten, M. T. M. Koper, *ChemCatChem* **2011**, *3*, 1176–1185.
[7] a) J. Qi, Le Xin, D. J. Chadderdon, Y. Qiu, Y. Jiang, N. Benipal, C. Liang, W. Li, *Appl. Catal. B* **2014**, *154–155*, 360–368; b) H. Wang, L. Thia, N. Li, X. Ge, Z. Liu, X. Wang, *Appl. Catal. B* **2015**, *166–167*, 25–31.
[8] a) D. Hiltrop, S. Cychy, K. Elumeeva, W. Schuhmann, M. Muhler, *Beilstein J. Org. Chem.* **2018**, *14*, 1428–1435; b) M. S. Ahmad, C. K. Cheng, R. Kumar, S. Singh, K. A. Saeed, H. R. Ong, H. Abdullah, M. R. Khan, *Electroanalysis* **2020**, *32*, 1139–1147.
[9] C. Dai, L. Sun, H. Liao, B. Khezri, R. D. Webster, A. C. Fisher, Z. J. Xu, *J. Catal.* **2017**, *356*, 14–21.
[10] C. A. Ottoni, S. G. da Silva, R. F. B. de Souza, A. O. Neto, *Ionics* **2016**, *22*, 1167–1175.
[11] P. J. Kulesza, I. S. Pieta, I. A. Rutkowska, A. Wadas, D. Marks, K. Klak, L. Stobinski, J. A. Cox, *Electrochim. Acta* **2013**, *110*, 474–483.
[12] a) A. Ashok, A. Kumar, J. Ponraj, S. A. Mansour, F. Tarlochan, *J. Electrochem. Soc.* **2018**, *165*, J3301–J3309; b) L. L. Carvalho, F. Colmati, A. A. Tanaka, *Int. J. Hydrogen Energy* **2017**, *42*, 16118–16126; c) B. Habibi, N. Delnavaz, *RSC Adv.* **2016**, *6*, 31797–31806; d) J. Han, Y. Kim, H. W. Kim, D. H. Jackson, D. Lee, H. Chang, H.-J. Chae, K.-Y. Lee, H. J. Kim, *Electrochem. Commun.* **2017**, *83*, 46–50; e) M. S. E. Houache, E. Cossar, S. Ntais, E. A. Baranova, *J. Power Sources* **2018**, *375*, 310–319; f) Q. Shao, J. Song, Y. Feng, X. Zhu, X. Huang, *ChemCatChem* **2018**, *10*, 3647–3652; g) D. E. Simpson, K. E. Juda, D. Roy, *Electrocatal.* **2018**, *9*, 86–101.
[13] V. L. Oliveira, C. Morais, K. Servat, T. W. Napporn, G. Tremiliosi-Filho, K. B. Kokoh, *J. Electroanal. Chem.* **2013**, *703*, 56–62.
[14] a) V. L. Oliveira, C. Morais, K. Servat, T. W. Napporn, G. Tremiliosi-Filho, K. B. Kokoh, *Electrochim. Act.* **2014**, *117*, 255–262; b) S. Cychy, S. Lechler, Z. Huang, M. Braun, A. C. Brix, P. Blümler, C. Andronescu, F. Schmid, W. Schuhmann, M. Muhler, *Chin. J. Catal.* **2021**, accepted; c) Y. Li, X. Wei, L. Chen, J. Shi, M. He, *Nat. Commun.* **2019**, *10*, 5335; d) X. Han, H. Sheng, C. Yu, T. W. Walker, G. W. Huber, J. Qiu, S. Jin, *ACS Catal.* **2020**, *10*, 12, 6741–6752; e) C. Liu, M. Hirohara, T. Maekawa, R. Chang, T. Hayashi, C.-Y. Chiang, *Appl. Catal. B* **2020**, *265*, 118543.
[15] C. H. Lam, A. J. Bloomfield, P. T. Anastas, *Green Chem.* **2017**, *19*, 1958–1968.
[16] a) J. Masa, I. Sinev, H. Mistry, E. Ventosa, M. de La Mata, J. Arbiol, M. Muhler, B. Roldan Cuenya, W. Schuhmann, *Adv. Energy Mater.* **2017**, *7*, 1700381; b) J. Masa, C. Andronescu, H. Antoni, S. Seisel, K. Elumeeva, S. Barwe, S. Marti-Sanchez, J. Arbiol, I. Sinev, B. Roldan Cuenya, M. Muhler, W. Schuhmann, *ChemElectroChem* **2019**, *6*, 235–240; c) J. Masa, S. Piontek, P. Wilde, H. Antoni, T. Eckhard, Y.-T. Chen, M. Muhler, U.-P. Apfel, W. Schuhmann, *Adv. Energy Mater.* **2019**, *9* 1900796; d) S. Möller, S. Barwe, S. Dieckhöfer, J. Masa, C Andronescu, W. Schuhmann, *ChemElectroChem* **2020**, *7*, 2680–2686.
[17] S. Barwe, J. Weidner, S. Cychy, D. M. Morales, S. Dieckhöfer, D. Hiltrop, J. Masa, M. Muhler, W. Schuhmann, *Angew. Chem. Int. Ed.* **2018**, *57*, 11460–11464; *Angew. Chem.* **2018**, *130*, 11631–11636.
[18] a) M. Sunitha, S. Asha, T. Ramachandran, *Ionics* **2020**, *26*, 1875–1884; b) J. Li, F. Luo, Q. Zhao, L. Xiao, J. Yang, W. Liu, D. Xiao, *Int. J. Hydrogen Energy* **2019**, *44*, 23074–23080.
[19] S. Cychy, D. Hiltrop, C. Andronescu, M. Muhler, W. Schuhmann, *Anal. Chem.* **2019**, *91*, 14323–14331.
[20] M. S. E. Houache, K. Hughes, R. Safari, G. A. Botton, E. A. Baranova, *ACS Appl. Mater. Int.* **2020**, *12*, 15095–15107.
[21] M. Fleischmann, K. Korinek, D. Pletcher, *J. Electroanal. Chem.* **1971**, *31*, 39–49.
[22] N.-T. Suen, S.-F. Hung, Q. Quan, N. Zhang, Y.-J. Xu, H. M. Chen, *Chem. Soc. Rev.* **2017**, *46*, 337–365.
[23] H. B. Tao, Y. Xu, X. Huang, J. Chen, L. Pei, J. Zhang, J. G. Chen, B. Liu, *Joule* **2019**, *3*, 1498–1509.
[24] J.-L. Lin, J. Ren, N. Tian, Z.-Y. Zhou, S.-G. Sun, *J. Electroanal. Chem.* **2013**, *688*, 165–171.

Manuscript received: May 30, 2021
Accepted manuscript online: June 11, 2021